



Trans. Nonferrous Met. Soc. China 22(2012) 1939-1946

Transactions of Nonferrous Metals Society of China

www.tnmsc.cn

Comparison of microstructures and mechanical properties between forging and rolling processes for commercially pure titanium

XU Chun¹, ZHU Wen-feng²

School of Materials Science and Engineering, Shanghai Institute of Technology, Shanghai 201418, China;
College of Mechanical Engineering, Tongji University, Shanghai 200092, China

Received 10 November 2011; accepted 18 August 2012

Abstract: In order to reveal the differences caused by forging and rolling process for titanium ingots, hot compression behavior, mechanical properties and the microstructures of forged billets and rolled ones were investigated in detail using Gleeble–1500 thermal mechanical simulator, universal testing machine and optical microscope (OM). The compression deformation experimental data of commercially pure titanium (CP-Ti) were mapped to be a T vs $\lg \dot{\varepsilon}$ diagram in which data fall into three distinct regions, i.e., three-stage work hardening, two-stage work hardening and flow softening, which can be separated by border lines at 17.5 and 15.4 for $\lg Z$, where Z represents the Zener–Hollomon parameter. The deformation twin is found to have higher Z-value corresponding to the work hardening region. The differences in microstructures and mechanical properties for two kinds of billets indicate that forged billet consists of deformation twins and some twin intersections, and many twins cross the grain boundaries. However, nearly no twins can be seen in the microstructure of billet formed by rolling under optical microscope (OM), but there are equiaxed and platelike grains. Tensile tests and Vickers hardness test indicate that yield strength, tensile strength and microhardness of the samples after forging are higher than those after rolling.

Key words: commercially pure titanium(CP-Ti); forging process; rolling process; microstructures; mechanical properties

1 Introduction

China has become one of the world's largest titanium producers and consumer countries with 54661 t sponge titanium production in 2010, about one-third of global production. Compared with the continuous rolling technology for titanium and titanium alloy used in heavy coil strips in Japan, Russia and America [1−3], process of vacuum arc remelting (VAR) ingot→forging and blooming→forging or rolling→slower cooling→ annealing→sheets and plates for titanium and titanium alloy has been still used in China, leading to the "big but not strong" situation for Chinese titanium industry.

Compared with forging process, rolling process is 500 RMB per ton cheaper in energy consumption. Furthermore, it is 10–20 times higher in productivity, twice higher in dimensional precision. In addition, there is not need for peeling and grinding processes after finish rolling. All these lead to the result that total cost of rolling production is 5000 RMB per ton lower than forming process [4].

For this reason, replacing forging with rolling for titanium and its alloy plates and sheets has become imperative to Chinese titanium industry, especially in utilizing the present equipment for producing steel sheet in order to reduce the cost of production further.

Although forging and rolling are both direct-compression-type deformation processes [5], there is difference in tool shape and movement, deformation-zone geometry and metal flow pattern. However, till now, little paper has been found to discuss yet. In this work, the ingots of Grade 2 commercially pure titanium (CP-Ti) is formed by high-speed forging and rolling to be billets, respectively. And their microstructure and mechanical properties are studied.

2 Experimental

2.1 Materials

Table 1 shows the composition of Grade 2 CP-Ti investigated in this study, which was mold cast into ingots of $d1040 \text{ mm} \times 2400 \text{ mm}$. It needs to note that there is a significant amount of Fe as an impurity.

Table 1 Chemical composition of experiment material (mass fraction, %)

| Fe | Si | C | Н | О | N | Ti |
|------|------|------|------|------|------|------|
| 0.30 | 0.15 | 0.10 | 0.05 | 0.15 | 0.05 | Bal. |

2.2 Procedures

2.2.1 Hot compression test

The middle part of the as-cast ingot of Grade 2 CP-Ti was machined into bar specimens with diameter of 8 mm and height of 15 mm using an electro-discharge machine. The specimens were compressed to deform using a Gleeble 1500 thermal simulator. Prior to hot compression, each specimen was heated at 10 °C/s up to 950 °C and held for 2 min to ensure a homogenous temperature distribution throughout the specimen. The deformation strain, temperature and strain rate were automatically controlled and recorded by the Gleeble 1500 thermal simulator system. Compression tests were conducted from 700 °C to 900 °C, every 50 °C interval varying the strain rates from 10, 20, 30 to 40 mm/min. The samples were deformed to a true compression strain of 0.60 and immediately cooled by water spraying to room temperature in order to maintain the deformed microstructures. The program is shown in Fig. 1.

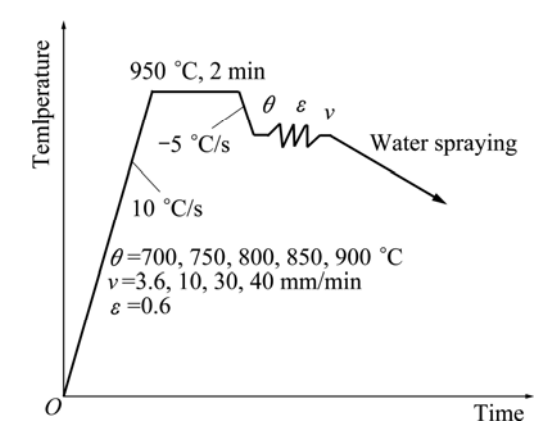


Fig. 1 Program for hot compression test

2.2.2 Sampling of forged and rolled billets

Two as-cast ingots were rolled on a 1500 mm blooming mill and forged via 39.2 kN high-speed forging pressure into billet of 1265 mm×200 mm. Two types of billets were intercepted from the middle part to prepare metallographic and tensile specimens, as shown in Fig. 2. Microstructure observations were conducted at the corresponding positions on the cross-sections of samples marked in Fig. 3. The samples to be examined with respect to their cross-sectional microstructure were cold mounted with resin. Cross sections of the samples were metallographically polished, ultrasonically cleaned in deionised water and pickled in Kroll's reagent (5 mL HF, 5 mL HNO₃ and 90 mL H₂O), and the microstructure

was observed under a light microscope. The microhardness (HV) was evaluated using a BUEHLER 1600–6406 Vickers diamond pyramidal indenter with a load of 98 mN.

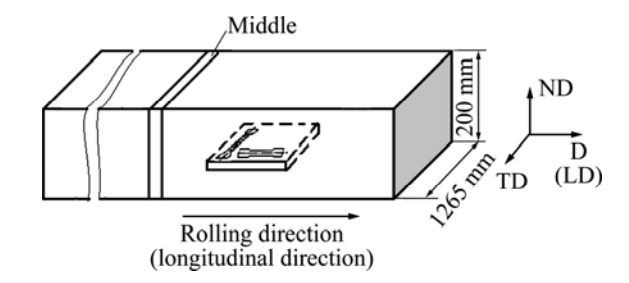


Fig. 2 Schematic diagram of specimen position for OM and tensile test in each billet

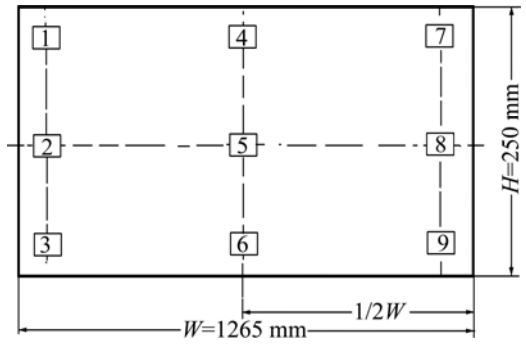


Fig. 3 Representative locations for OM observation of cross-sections of samples

Mechanical properties were evaluated after forging and rolling processes. Tensile tests were performed at room temperature using a universal testing machine ZWICK-100. Cylindrical samples (see Fig. 4) with a gauge section of 10 mm in diameter and 50 mm in length were machined from the Ti billets. A displacement rate of 1 mm/min was used for all tests. Yield strength, ultimate strength, and elongation to failure were measured. To measure the anisotropy of tensile strength, the samples were cut from the transverse as well as longitudinal sections, as shown in Fig. 2.

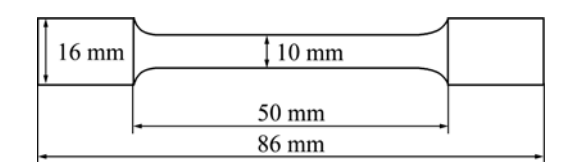


Fig. 4 Geometry of cylindrical tensile testing specimen

3 Results

3.1 True stress—strain curves

Figure 5 shows the stress—strain curves for CP Ti from the uniaxial compression tests from 700 to 900 °C with 50 °C interval and strain rates of 3.6, 10, 30 and

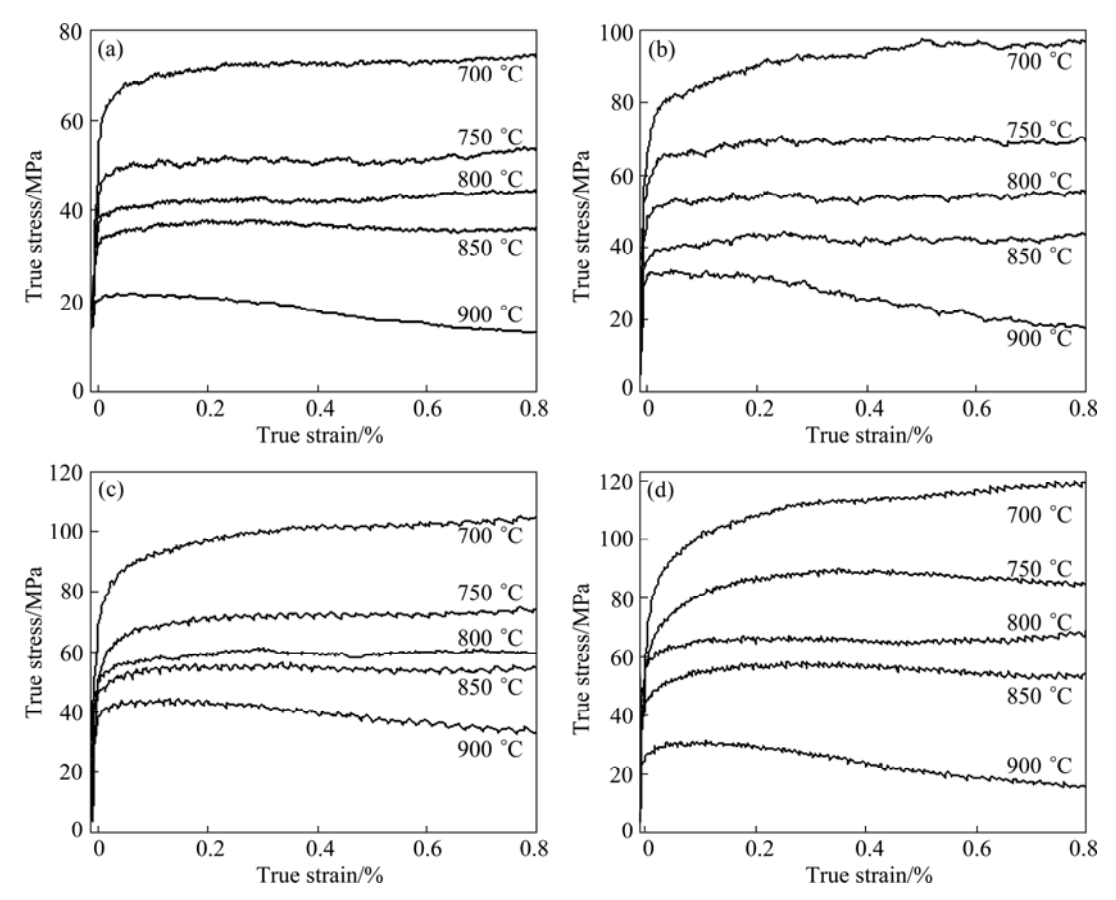


Fig. 5 Stress—strain curves showing flow stress of CP Ti in compression at various temperatures and strain rates: (a) 3.6 mm/min; (b) 10 mm/min; (c) 30 mm/min; (d) 40 mm/min

40 mm/min. As expected, the flow stress is sensitive to both temperature and strain rate. It decreases with increasing temperature, or with decreasing strain rate. At the same temperature, the flow stress increases with increasing strain rate. When deforming at 900 °C, the material exhibits a slight transitional drop in flow stress, indicating thermal softening. However, at 700 °C and strain rate from 10 to 40 mm/min, or at 3.6 mm/min and below 800 °C, the stress—strain curves show a work hardening character. At 10, 30 and 40 mm/min and from 750 to 950 °C, or at 3.6 mm/min and temperatures of 800 and 850 °C, the flow stress shows a steady state flow at true strains from 0.2 to 0.8.

Data in Fig. 5 were analyzed by fitting each experimental curve with a polynomial expression and taking its derivative with respect to strain in order to obtain the work hardening rate. Then, the work hardening rate was plotted against flow stress, as shown in Fig. 6. By inspecting these plots, it was found that the curves could be divided into three groups: three-stage work hardening; two-stage work hardening; and flow softening.

3.2 Deformation condition map

Figure 6 is constructed by plotting all data into a

map with $\lg \dot{\varepsilon}$ and temperature as coordinate axis. All data consistently fall into three domains. At low temperatures (700 °C) and any strain rate, or lower temperatures and higher strain rates, the domain of three-stage work hardening is located. At higher temperatures, the domain for two-stage work hardening is found and at high temperatures (900 °C) and any strain rate, the domain of flow softening is found. Whenever the combined effect from changes in temperature, T, and strain rate, $\dot{\varepsilon}$, is considered, the Zener–Hollomon parameter, T, is a natural choice of parameter. It is defined as:

$$Z = \dot{\varepsilon} \exp(\frac{Q}{RT}) \tag{1}$$

where R is the gas constant and Q is the activation energy. In the present study, the value of Q is taken from the result for CP Ti reported by XU and ZHU [6], 162 kJ/mol. Thus, by using Eq. (1) it is possible to draw contour lines for different Z-values in Fig. 7. By testing different Z-values, it was found that two border lines could be drawn to divide the map into three regions, i.e., three-stage work hardening, two-stage work hardening and flow softening, almost perfectly consistent with the experimental information. The approximate values of the

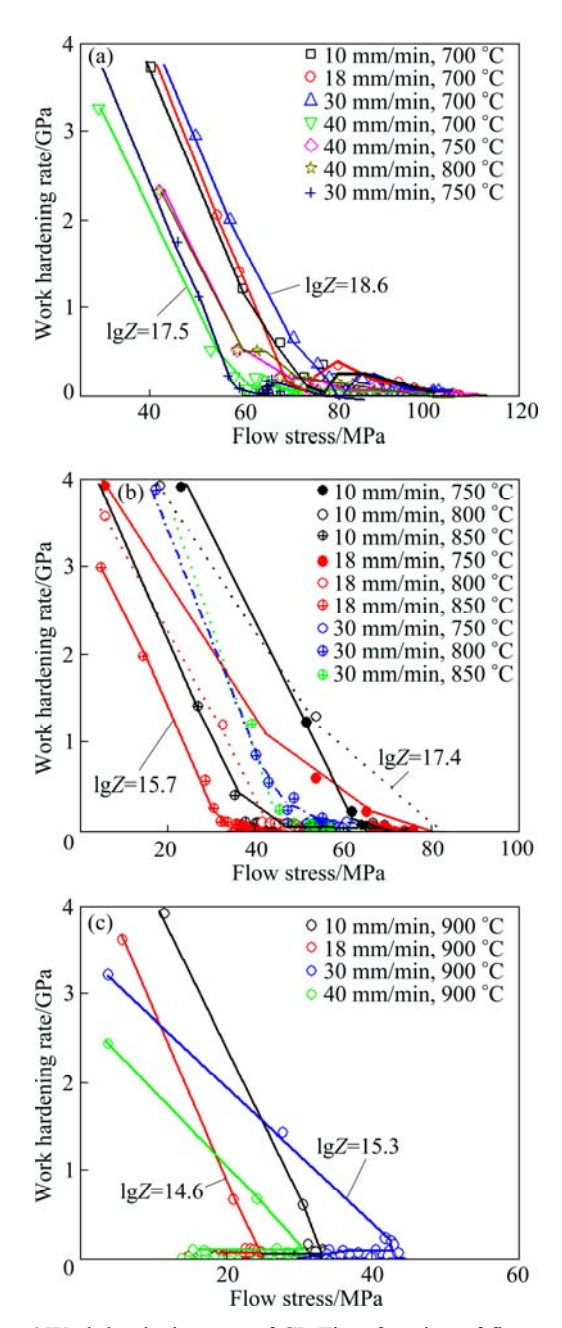


Fig. 6 Work hardening rate of CP-Ti as function of flow stress for three-stage work hardening (a), two-stage work hardening (b) and flow softening (c)

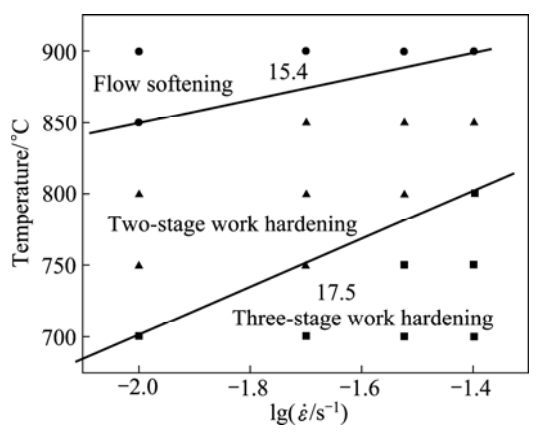


Fig. 7 Deformation condition map of CP-Ti

border lines are, $\lg Z=15.4$ and 17.5, respectively, as indicated in Fig. 7. Three-stage work hardening is located in higher *Z*-values and flow softening is in lower *Z*-values.

After producing the curves of three-stage work hardening in Fig. 6(a), the microstructures of the samples were examined after full deformation i.e., a true strain of 0.8. The optical micrograph of the sample deformed at 700 °C and 40 mm/min is illustrated in Fig. 8(a). Elongated coarse grains are mixed with refined grains. In the coarse grains, deformation twinning with common orientation is observed.

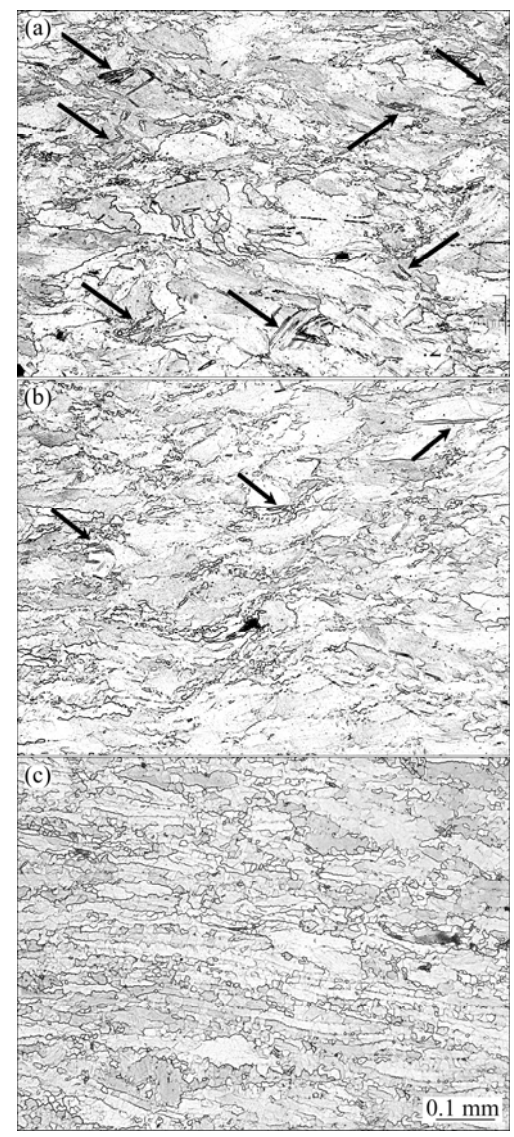


Fig. 8 Microstructures of CP Ti deformed in compression at various temperatures and strain rates: (a) 700 °C, 40 mm/min; (b) 850 °C, 10 mm/min; (c) 900 °C, 10 mm/min (Black arrows mark some of the twins)

The optical micrographs of the samples in two-stage work hardening curve in Fig. 6(b) were observed after a total strain of 0.8. Inhomogeneous microstructures, similar to those in Fig. 8(a), appear. However, fewer

deformation twins are observed. The optical micrograph of the sample deformed at 850 °C and 10 mm/min is shown in Fig. 8(b).

In Fig. 6(b), the inhomogeneous microstructure without deformation twinning is found in the optical micrograph of the sample in flow softening curve. It is different from that in Fig. 8(a) or 8(b). The optical micrograph of the sample deformed at 900 °C and 10 mm/min after a total strain of 0.8 is shown in Fig. 8(c).

3.3 Microstructural characterization of forging and rolling billets

The microstructural features corresponding to various deformation regimes are shown in Figs. 9 and 10. Deformation twins and some twin intersections are clearly displayed in subsurface positions in cross sections of samples after forging, as shown in Figs. 9(a), (c), (d), (f), (g) and (i), and those locations are marked in Fig. 3 as 1, 7, 2, 8, 3 and 9, respectively. Many twins cross the grain boundaries, and nonuniform distribution of twins and their intersections occurred inside many grains. But then its inner position consists of equiaxed α grains and some elongated α grains, which are shown in Figs. 9(b), (e) and (h), and essentially no twins are seen in central position shown in Fig. 9(e) and the locations are marked

5 in Fig. 3.

Microstructures after rolling are shown in Fig. 10. Compared with microstructures after forging, the features are obviously different. Essentially no twins are seen, and equiaxed grains clearly appear at four corner positions of rolling sample, which are shown in Figs. 10(a), (c), (g) and (i), and the locations are marked in Fig. 3 as 1, 7, 3 and 9, respectively. The equiaxed grains are uniform, the grain boundaries are smooth, and there are many small grains. Some plate-like α grains are found in inner positions except four corner positions, which are shown in Figs. 10(b), (e), (f) and (h), and the locations are marked in Fig. 3 as 4, 5, 8 and 6, respectively.

3.4 Microhardness of forging and rolling billets

Table 2 shows average microhardness of the corresponding positions on the cross sections of samples marked in Fig. 3. At each location, the microhardness was measured 5 times. The average values are shown in Table 2. It could be seen that the hardness distribution on the cross section is inhomogeneous in two different processes. Although the average microhardness in the forged section is higher than that in the rolled ones, the scattering of the measured value is more uniform in the forging than in the rolling.

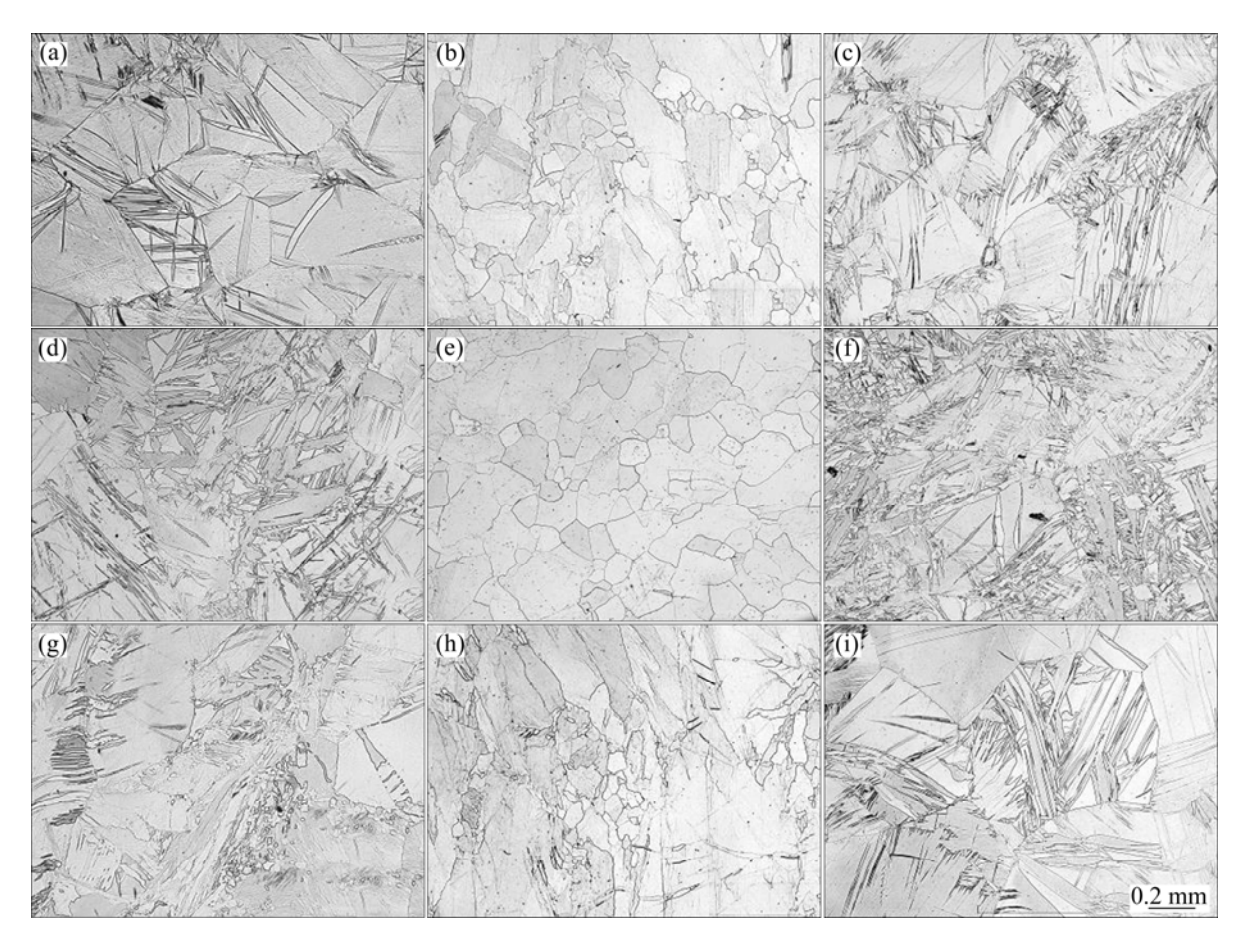


Fig. 9 As-forged microstructures of sampling positions in Fig. 3: (a) 1; (b) 4; (c) 7; (d) 2; (e) 5; (f) 8; (g) 3; (h) 6; (i) 9

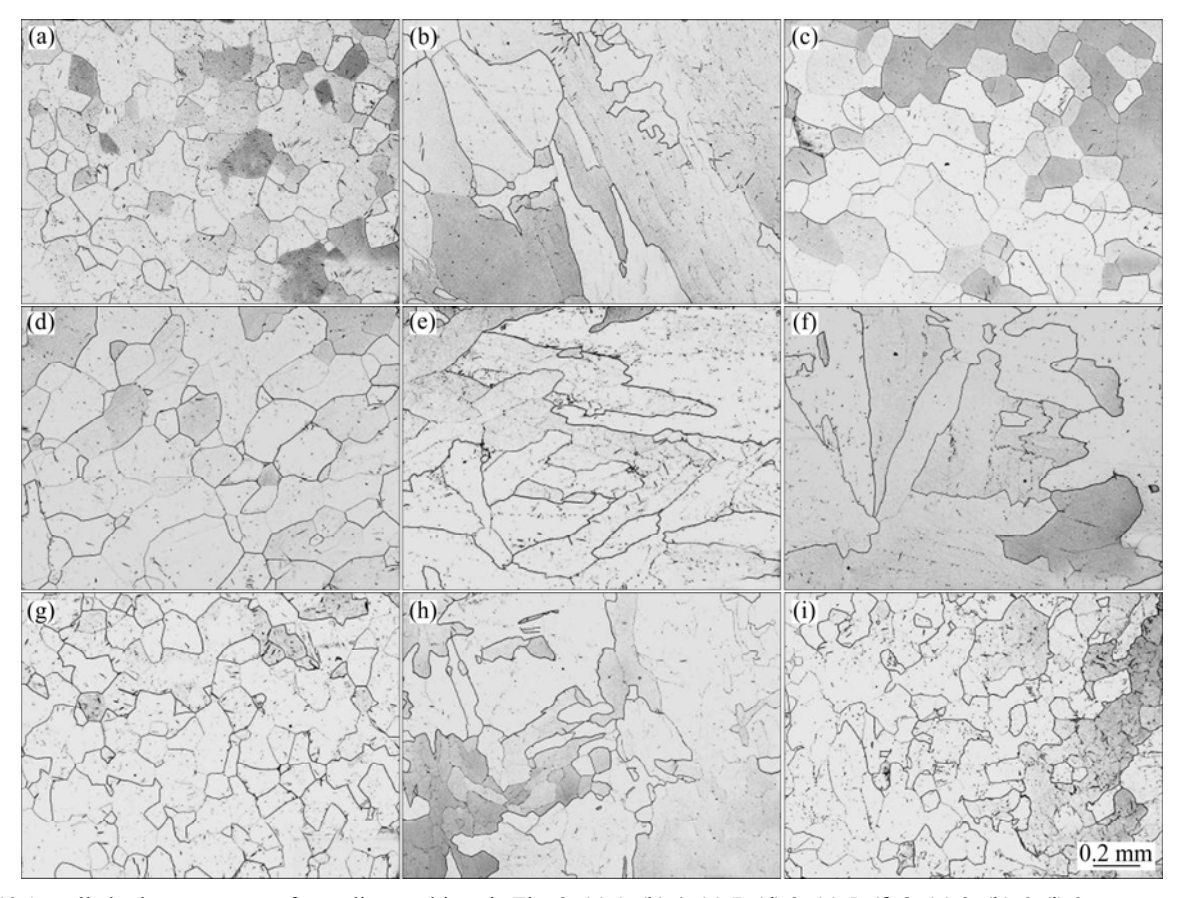


Fig. 10 As-rolled microstructures of sampling positions in Fig. 2: (a) 1; (b) 4; (c) 7; (d) 2; (e) 5; (f) 8; (g) 3; (h) 6; (i) 9

Table 2 Microhardness measured of corresponding positions on cross sections of samples as marked in Fig. 3

| State | HV ₁₀ /MPa | | | | | | | _ A | | |
|-----------|-----------------------|-----|-----|-----|-----|-----|-----|-----|-----|-----------|
| | 1 | 2 | 3 | 4 | 5 | 6 | 7 | 8 | 9 | - Average |
| As-forged | 156 | 183 | 191 | 193 | 160 | 153 | 167 | 204 | 157 | 172.4 |
| As-rolled | 160 | 156 | 134 | 149 | 111 | 208 | 148 | 134 | 190 | 150.8 |

3.5 Mechanical properties of forged and rolled billets

Tensile tests were conducted on cylindrical samples with gauge dimensions of 10 mm in diameter and 50 mm in length. The longitudinal axis of the sample coincided with that of the billets. Typical strain—stress curves of CP-Ti in two different processes are shown in Fig.11. The yield and ultimate strength values of CP-Ti billet produced by forging process are slightly higher than those produced by rolling process, although the rolling generated finer equiaxed grains. It is because more twins and dispersed precipitates in the forged microstructure may somewhat increase the tensile strength.

Elastic modulus, yield strength, ultimate strength, and elongation to failure are listed in Table 3. Each value is the average value measured after three tensile tests. The yield strength and ultimate strength of the forged CP-Ti are higher than those of the rolled one. Besides, the yield and ultimate strength values of the forged CP-Ti in longitudinal and transverse directions are

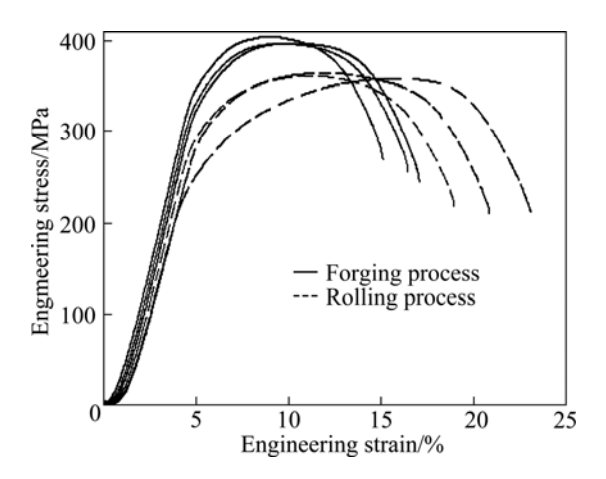


Fig. 11 Typical tensile stress—strain curves for CP-Ti billets

almost the same. However, the strengths in longitudinal direction are obviously higher than those in transverse one for the rolled CP-Ti. And the ductility of 24%–37% elongation is higher than that of the forged one. So, it is

seen that the rolling process produces CP-Ti billets with anisotropic mechanical properties.

Table 3 Mechanical properties of CP-Ti billets by two different forming processes

| Route | | Elastic modulus/ GPa | Yield strength/ MPa | Ultimate strength/ MPa | Elongation/ |
|---------|----|----------------------------|---------------------------|------------------------------|-------------|
| Rolling | LR | 4.2 | 282 | 372 | 37 |
| | TR | 5.3 | 305 | 382 | 24 |
| Forging | LR | 7.1 | 363 | 396 | 25 |
| | TR | 7.1 | 364 | 399 | 22 |

4 Discussion

Figure 7 shows that the deformation condition map of CP-Ti can be divided into three regions, namely, three-stage work hardening, two-stage work hardening and flow softening, which can be separated by Z-values. Three-stage work hardening is located in region higher than $\lg Z=17.5$, and flow softening is in region lower than $\lg Z=15.4$. Figure 8(a) indicates that the deformation twins are more profuse at higher Z-value regions, such as three-stage work hardening and two-stage work hardening. Twin exhibits a strong dependence on the deformation temperature and strain rate. Because CP-Ti is a typical HCP metal, its deformation begins with slipping. However, since the number of active slip systems is less for BCC and FCC metals, deformation twinning begins to play a vital role, even at a low strain and a low deformation temperature, such as being deformed at 700 °C and 3.6 mm/min, i.e., at higher Z-values. As known from the results reported by SALEM et al [7], a profuse deformation twinning is the reason leading to the second stage of the three-stage work hardening.

LI et al [8] has revealed that the effective interfacial heat transfer coefficients (IHTCs) from hot rolling are substantially higher than those from hot forging under nearly the same conditions of specimen thickness, deformation temperature, reduction and speed. The temperatures at the subsurface (2 mm below the top surface of the specimen) drop earlier and more rapidly than the central ones during hot forging [9]. So, a large temperature difference appears between the centre and the subsurface of sample during forging deformation. The temperatures at the subsurface of forging sample are much lower, but the central ones still keep higher temperature. In other words, the subsurface is located in work hardening region and the central is in flow softening region during forging deformation, which explains why deformation twins are more profuse in subsurface area of cross sections of forging sample. On the other hand, in Fig. 9, there is a small temperature difference between the centre and the subsurface of sample during rolling deformation. The temperatures in difference areas of rolled sample are still high. So, the subsurface areas of rolling sample are located in flow softening region. It is why no twins appear in samples after rolling in Fig. 10. But some plate-like α grains could be observed in inner positions except four corners. Obviously, the cooling rate of corners is higher than other positions. It was reported that long plate-like α grains could appear at a slow cooling rate [6].

Figures 9 and 10 clearly show the obvious different microstructural features in two forming processes. The forged billet has microstructures consisting of deformation twins and some twin intersections, and many twins cross the grain boundaries. But the rolled billet consists of equiaxed and plate-like grains and there are no twins. In Refs. [10–12], the twin boundaries could prevent dislocation from slipping and result in the strengthening effect. So the strength of the forged CP-Ti billet is higher than that of the rolled one.

5 Conclusions

- 1) The deformation behavior of CP-Ti can be divided into three types, namely, three-stage work hardening, two-stage work hardening and flow softening. When the experimental data are mapped in a T vs $\lg \dot{\varepsilon}$ diagram, the present and previous data fall into three distinct regions which can be successfully separated by border lines at 17.5 and 15.4 for $\lg Z$, where Z represents the Zener–Hollomon parameter.
- 2) There are quite different microstructural features between forging and rolling processes. The forged billet has microstructures consisting of deformation twins and some twin intersections with many twins cross the grain boundaries. The rolled microstructures consist of both equiaxed and plate-like grains, while no twins are seen in an optical microscope. It is because of the quite lower temperatures at the subsurface than the central ones during hot forging, which results in hot deformation in subsurface into work hardening regions.
- 3) The strength of the forged CP-Ti is higher than that of the rolled one, and the elongation of the forged sample is lower than that of the rolled one, due to more twin crystals in the forged microstructure. The forged billet has homology yield and ultimate strength along both longitudinal and transverse directions, but those of the rolled one are obviously different.
- 4) There is non-uniform microhardness distribution on all billets, but the microhardness of the forged billet is higher than that of the rolled one, and the scattering of the measured value is more uniform in the forged billet than that in rolled one.

References

- CHEN Yong-hong. Elementary analysis of the current situation of the titanium industry in USA, Japan and China [J]. Titanium Industry Progress, 2005, 22(4): 12–14. (in Chinese)
- [2] WU Quan-xing. Present situation and prospect of Ti mill products in Japan [J]. Rare Metals Letters, 2004, 23(1): 11–14. (in Chinese)
- [3] WANG Xiang-dong, LU Fu-sheng, JIA Hong, HAO Bin, MA Yun-feng. 30-year development of china titanium industry [J]. Titanium Industry Progress, 2009, 26(3): 1–6. (in Chinese)
- [4] CHEN Xi-qiang. The effects of rolling process on microstructures and properties of the commercial pure titanium [J]. Iron Steel Vanadium Titanium, 2009, 30(4): 16–20. (in Chinese)
- BOEHLERT C J. The effects of forging and rolling on microstructure in O+BCC Ti-Al-Nb alloys [J]. Materials Science and Engineering A, 2000, 279: 118-129.
- [6] XU Chun, ZHU Wen-feng. Transformation mechanism and mechanical properties of commercially pure titanium [J]. Transactions of Nonferrous Metals Society of China, 2010, 20(11):

- 2162-2167.
- [7] SALEM A A, KALIDINDI S R, DOHERTY R D. Strain hardening regimes and microstructure evolution during large strain compression of high purity titanium [J]. Scripta Materialia, 2002, 46: 419–423.
- [8] LI Y H, SELLARS C M. Comparative investigations of interfacial heat transfer behavior during hot forging and rolling of steel with oxide scale formation [J]. Journal of Materials Processing Technology, 1998, 80–81: 282–286.
- ZENG Zhi-peng, ZHANG Yan-shu, STEFAN J. Deformation behavior of commercially pure titanium during simple hot compression [J]. Materials and Design, 2009, 30: 3105–3111.
- [10] NAGASEKHAR A V, CHAKKINGAL U, VENUGOPAL P. Candidature of equal channel angular pressing for processing of tubular commercial purity-titanium [J]. Journal of Materials Processing Technology, 2006, 173: 53–60.
- [11] STOLYAROV V V, ZHU Y T, LOWE T C, ISLAMGALIEV R K, VALIEV R Z. A two step SPD processing of ultrafine-grained titanium [J]. Nanostructured Materials, 1999, 11: 947–954.
- [12] SEMIATINA S L, DEL D P. Equal channel angular extrusion of difficult-to-work alloys [J]. Materials and Design, 2000, 21: 311–322.

锻造与轧制工艺对纯钛组织与力学性能的影响

徐春1、朱文峰2

- 1. 上海应用技术学院 材料科学与工程系, 上海 201418;
 - 2. 同济大学 机械工程学院, 上海 200092

摘 要:为了研究锻造和轧制这两种开坯工艺对纯钛板坯组织和性能的影响,在 Gleeble—1500 热模拟实验机上进行热压缩实验,通过单向拉伸实验测试锻造和轧制后板料的力学性能,在光学显微镜下观察采用两种开坯工艺加工后的显微组织。以变形温度(T)和应变速率的对数(lg é)为坐标作图,根据 lg Z 值的斜率,即 15.4 和 17.5,能够将纯钛塑性变形分成 3 个区,即三阶段加工硬化区、二阶段加工硬化区和流动软化区。在较高 Z 值的两种加工硬化区会有变形孪晶出现。两种开坯生产工艺对纯钛板坯组织和性能的影响主要体现在:锻坯微观组织出现变形孪晶,即晶内出现交叉孪晶,还有一些孪晶横穿晶界。然而,在轧坯中没有发现孪晶,其微观结构主要为等轴晶和板条状晶粒。拉伸实验和显微硬度测试结果显示,锻坯的屈服和抗拉强度及显微硬度均高于轧坯的。

关键词: 纯钛; 锻造工艺; 轧制工艺; 显微组织; 力学性能

(Edited by YANG Hua)